Combination of Analytical Model and Finite Element Method for Designing High Voltage Shunt Reactors

Dung Dang Chi[1,*], Nam Phan Hoai[2], Hung Bui Duc[1], Tu Pham Minh[1], Hieu Dinh Thi Trung[3]
and Vuong Dang Quoc[1]

[1]*Department of Electrical Engineering, School of Electrical and Electronic Engineering, Hanoi University of Science and Technology*
[2]*Faculty of Electrical Engineering, University of Economic and Technical Industries*
[3]*Faculty of technology and Engineering, University of Hai Duong*
*Corresponding author: dung.dangchi@hust.edu.vn

Abstract

Presently, shunt reactors (SRs) play a crucial role in addressing power quality issues. These SRs are designed to mitigate the reactive power in the system, manage high voltages, suppress power frequency fluctuations, regulate over-voltage, eliminate excitation in generators and dynamically compensate for transmission line power charges. The application of the finite element method (FEM) in the design of SRs has been recently presented by many researchers, particularly in both no-load and full-load conditions. However, its utilization in the manufacturing of electrical SRs remains relatively limited. In this study, it is split into two main steps. First, an analytical design is proposed to define the desired parameters with affects of different flux air gaps. Then, a finite element approach is introduced to simulate magnetic field quantities (such as inductance, fringing flux, magnetic flux density, electromagnetic force, current, voltage) of the SRs. The development of the methods is validated on the practical SR of 16 MVar, and a voltage of 500/√3.

Keywords: Shunt reactors, fringing flux, leakage flux, flux air gap, analytic model, finite element method

1. Overview

To prevent overvoltage phenomena and maintain stable voltage at the end of transmission lines with a voltage rating of 110kV or higher during light or no-load system operation, shunt reactors (SRs) are employed to absorb and balance reactive power. Recently, many researchers have conducted numerous studies on shunt reactors, as follows:

In reference [1], a research group utilized the finite element method (FEM) to compute and analyze the reactance of SRs to establish the relationship between the total reactance and the leakage reactance between core blocks. In reference [2], an analytical method was developed to calculate the geometric parameters of the core and winding of SRs. The obtained results were compared to the FEM. In reference [3], [4], the authors applied the FEM to provide a solution for reducing losses caused by eddy currents in the winding of SR by optimizing the air gap along the winding. This paper also investigated the fringing and leakage fluxes around the air gaps. In reference [5], the authors presented a method for calculating the air gap impedance in the magnetic circuit of the shunt reactor through the "Schwarz-Christoffel" transformation.

Despite many researchers have applied the FEM for computation, analysis, and modeling of the electrical parameters of SRs, assessing the impact of electromagnetic forces on the core block, however it still remains a significant challenge for researchers and reactor manufacturers when considering the flux air gaps on the output parameters of SRs.

In this study, it is split into two main steps. First, an analytical design is proposed to define the desired parameters with affects of different flux air gaps. Then, a finite element approach is developed to simulate inductances, leakage and fringing fluxes, magnetic flux density and electromagnetic force with different flux air gaps. The development of the methods is validated on the practical SR of 16 MVar, and a voltage of 500/√3.

In the first section, the problem statement is introduced, as previously described. The second section shows the modeling of a SR with one flux air gap. The third section presents the analtyical approach to defined the required parameters of the SR. The fourth section develops the FEM with magnetic vector potential formulations to calcualte electromagnetic parameters. The fifth section gives a practical test of SR to validate the theory developed by the two proposed methods. The final section summarizes the obtained results.

2. Model of a single phase SR

The model of single-phase SR used in the transmission grid system is depicted in Figure 1 [3]. To reduce the fringing and leakage fluxes appearing in the vicinity of core blocks and also avoid saturation of the SR, the core blocks usually divide into several flux air gaps with significant lengths as already presented in [4]. However, the extensive length of these air gaps results in the presence of significant leakage flux and stray magnetic flux around the air gaps, causing the the main magnetic flux to decrease. Therefore, to mitigate this leakage flux component, instead of using a single flux air gap with a

large thickness, it is necessary to divide the air gap into smaller flux air gaps with maintaining the total length of the gaps constant as shown in Figure 1. This approach increases the reluctance around the air gap region and reduces the leakage and fringing fluxes. However, dividing a large flux air gap into smaller flux air gaps implies segmenting a long core block into smaller sections, which in turn impacts the structural integrity of the magnetic circuit SR. The flux air gaps along the core blocks depend on the key parameters of the reactor, such as reactive power, magnetic flux density, inductance, energy stored in the winding space and the flux air gaps. These air gaps can be determined using an analytical model
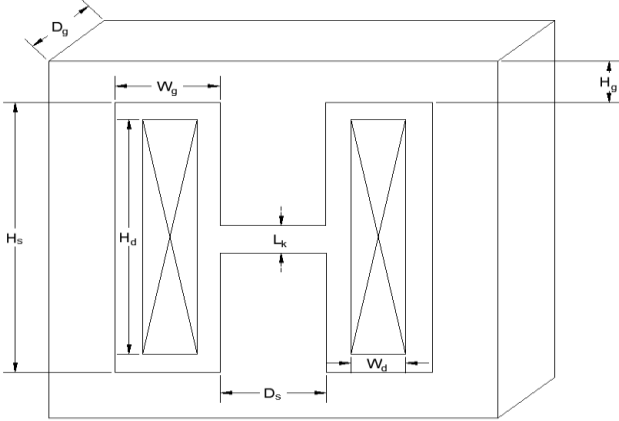
Figure 1. Model of a single phase SR [3].
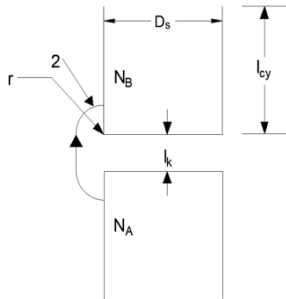
Figure 2. Fringing flux for an air gap along the core block [4].

3.   Analytical approach

3.1. *Computation of fringing flux of the SR*

In this part, the main parameters of the single phase SR are defined via an analytica approach. Based on Figure 2, for a single flux air gap along the core block is considered. The magnetomotive force (MMF) is defined via the Ampere law, i.e., [2]-[5]:

$$F = \oint H.\,dl = H.\,(l_k + \pi.\,r) \tag{1}$$

where H is magnetic field intensity, l_k is the flux air gap thickness of the core block and r is the radius of fringing/leakage flux. The magnetic flux density (B) can be computed as:

$$B = \frac{\mu_o.\,F}{(l_k + \pi.\,r)} \tag{2}$$

The fringing flux ($\phi_{\text{fring*}}$) around the single flux air gap of core block is then defined:

$$\phi_{\text{fring*}} = \frac{\int B dS}{F} = \int_0^{\frac{l_{cy}}{2}} \frac{\mu_o}{(l_k + \pi.\,r)}d_c d_r$$
$$= \frac{\mu_o.D_s}{\pi}\ln\left(1 + \frac{\pi.\frac{l_{cy}}{2}}{l_k}\right) \tag{3}$$

It should be noted that the shape of core is the cylinder, for that it gets $d_c = \pi D_s$. For that, the equation (3) becomes as

$$\phi_{\text{fring*}} = \mu_o.\,D_s.\ln\left(1 + \frac{\pi.\,l_{cy}}{2.\,l_k}\right) \tag{4}$$
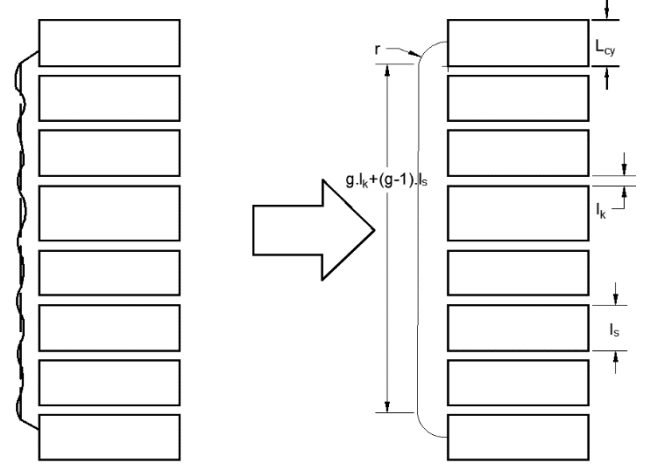
Figure 3. Model of several flux air gaps along the core blocks.

For the several flux air gaps as pointed out in Figure 3, the MMF is now defined as [6]-[10]:

$$F = \oint H.\,dl = H.\,((g-1)l_s + gl_k + \pi.\,r), \tag{5}$$

where l_s is the thickness of core block and g is the lenght of fringing flux and l_k is the thickness of flux air gap. In the same way, the term B can be calculated:

$$B = \frac{\mu_o.\,F}{((g-1)l_s + gl_k + \pi.\,r)} \tag{6}$$

The fringing flux ($\phi_{\text{fring**}}$) around the several flux air gaps is then defined:

$$\phi_{\text{fring**}} = \frac{\int B dS}{F} = \int_0^{l_{cy}} \frac{\mu_o}{((g-1)l_s + gl_k + \pi.\,r)}\pi D_s d_r$$
$$= \frac{\mu_o.\,D_c}{\pi}.\ln\left(1 + \frac{\pi.\,l_{cy}}{(g-1)l_s + gl_k}\right) \tag{7}$$

3.2. *Determination of main dimensions of the SR*

In this part, the single phase SR of 16 MVar, the voltage (U) of $500/\sqrt{3}$, frequency of 50 Hz, is considered. The model of this SR is already given in Figure 1. The electromagnetic force (EMF) and the electric current can be defined as [3], [6]-[12]:

$$E = \left(\frac{2\pi}{\sqrt{2}}\right).f.\,N.\,\phi_m = \left(\frac{2\pi}{\sqrt{2}}\right).f.\,N.\,B_m.\,A_k \tag{8}$$

$$I = \frac{.\,R_g}{N} = \left(\frac{1}{\sqrt{2}}\right)\frac{B_m.\,l_g}{\mu_0.\,N}, \tag{9}$$

where:
- ϕ_m is the maximum magnetic flux,
- B_m is the maximum flux density,
- A_k is the area of the air gap,
- l_g is the length of the air gap,

- R_g air gap reluctance and air permeability.
- μ_0 is the permeability an N is the turn number.

Based on the equations (8) and (9), the volume (V_k) of the flux air gap is determined as:

$$V_k = A_k \cdot l_k = \frac{Q}{\frac{\pi}{\mu_0} \cdot f \cdot B_m^2}. \tag{10}$$

The dimension of core block can be defined via the area of the flux air gap, that is

$$D_c = \sqrt{\frac{4 \cdot A_k}{\pi}} \tag{11}$$

From the equation (11), the deep yoke (D_y) and the high yoke (H_y) of core block can be then defined as:

$$D_y = D_c, \quad H_y = \frac{A_k}{2 \cdot D_y}. \tag{12 a-b}$$

The inductance of winding can be calculate via the expression [3]-[5]:

$$L = N^2 \cdot \mu_0 \cdot \left(\frac{A_k}{l_k}\right) = \left(\sqrt{\frac{L}{\mu_0 \cdot \left(\frac{A_k}{l_k}\right)}}\right)^2 \cdot \phi_g \tag{13}$$

The magnetic conducting taken the fringing flux into account is expressed as

$$\phi_{g_f} = \frac{\phi_g + \phi_{fring*} + g\phi_{fring**}}{g} \tag{14}$$

The turn number is finally written via the term, i.e

$$N = \sqrt{\frac{L}{\phi_c + \phi_{g_f}}} \tag{15}$$

Based on the analytic theory developed as above, the analytic results of the proposed SR of 16 MVar are given in Table 1:

Table 1. Analytical results

Parameters	Symbol	Value
Reactive power	Q (MVAr)	16
Rated voltage	U (kV)	$500/\sqrt{3}$
Rated current	I (A)	55.25
Total inductance	L_{total} (H)	16.6
Fringing inductance	$L_{fringing}$ (H)	5.15
Gap inductance	L_{gap} (H)	10.27
Core dimension	D_s (mm)	572
Height of core	Hs (mm)	1534
Total air gap	l_k (mm)	256
Turn number	N (turn)	2853
Width of winding	Wd (mm)	211
Height of winding	Hd (mm)	1264
Gaps	g	5

4. Finite element method

4.1. Maxwell's equation

In this contex, the FEM is proposed to simulate and compute the inducances, magnetic field density and electromagnetic forces with the different flux air gaps in the proposed SR. The general set of Maxwell's equations defined in a studied domain Ω and its boundary ($\partial\Omega \equiv \Gamma$) are given as [13]-[18]:

$$\text{curl } e = -\partial_t b \quad \text{in } \Omega, \tag{16}$$
$$\text{curl } h = j_s \quad \text{in } \Omega_s, \tag{17}$$
$$\text{div } b = 0 \quad \text{in } \Omega, \tag{18}$$

where fields of e, b, h, j_s are respectively the electric field (V/m), magnetic flux density (Wb), magnetic field intensity (A/m) and electric current density (A/mm^2). These fields satify function spaces defined inthe Tonti's diagram [11], that is, $e \in H_e(\text{curl}; \Omega)$, $j \in H(\text{div}; \Omega)$, $h \in H_h(\text{curl}; \Omega)$, $b \in H_e(\text{div}; \Omega)$. It should be noted that $\Omega = \Omega_c \cup \Omega_c^C$, where Ω_c is the conductive domain and Ω_c^C is the non conductive domain.

The equations from (16) to (18) are solved with the behavior laws and the boundary conditions (BCs), i.e.,

$$b = \mu h, \quad j = \sigma e. \tag{19 a-b}$$
$$n \cdot B|_{\Gamma_e} = 0, \quad n \times H|_{\Gamma_h} = 0, \tag{20 a-b}$$

where parameters μ and σ are respectively the permeability and electric conductivity, and n is the normal unit.

The magnetic flux density b is presented via the magnetic vector potential (a), i.e, $b = \text{curl } a$. Thus, the equation (16) is presented via the electric scalar potential (υ)

$$e = -j\omega A - \text{grad}\upsilon. \tag{21}$$

But, in Ω_c, the υ is fixed to be zero [18].

4.2. Weak finite element formulations

The weak formulations for magnetic vector potential (a) is written based on the Maxwell's equations from (16) –(17), behavior laws (19 a-b), BCs (20a-b) and equation (22) [18]:

$$\int_\Omega \mu^{-1}\text{curl } a \cdot \text{curl } w' d\Omega + j \int_{\Omega_c} (2\pi f \sigma a \cdot w') d\Omega_c$$
$$+ \int_{\Omega_c} (\sigma \text{grad}\upsilon \cdot w') d\Omega_c + \int_{\Gamma_h} (n \times H) \cdot w' d\Gamma_h$$
$$= \int_{\Omega_s} (j_s \cdot w') d\Omega_s, w' \in H_e^0(\text{curl}; \Omega), \tag{22}$$

where w' is the test function given in a function space $H_e^0(\text{curl}; \Omega)$.

The trace of magnetic field is achievable, especially under conditions such as a homogeneous Neumann BC. This is exemplified by imposing a symmetry condition like "zero crossing current" or considering a perfect magnetic wall with infinite magnetic permeability. When the applied voltage is considered as global quantities, the υ can be defined as:

$$\upsilon = \sum_i V_i v_{s,i} \tag{23}$$

where $v_{s,i}$ is a basic function υ and V_i is the voltage drop on the electrodes [18].

By substituting (23) into (22), the equation (22) becomes:

$$\int_\Omega \mu^{-1}\text{curl } a \cdot \text{curl } w' d\Omega + j \int_{\Omega_c} (2\pi f \sigma a \cdot w') d\Omega_c$$

$$+\int_{\Omega_c}\left(\sigma\mathrm{grad}\sum_i V_i v_{s,i}\cdot\mathbf{w}'\right)d\Omega_c+\int_{\Gamma_h}(\boldsymbol{n}\times\mathbf{H})\cdot\mathbf{w}'d\Gamma_h$$
$$=\int_{\Omega_s}(\mathbf{j_s}\cdot\mathbf{w}')d\Omega_s\,,\mathbf{w}'\in H_e^0(\mathrm{curl};\Omega),\quad(24)$$

4.3. Discretization of fields

The fields $\boldsymbol{a}$ and υ in the equation (24) are discreted via the edge and node elements, i.e., [13].

$$\mathbf{a}=\sum_{e\in E(\Omega_c)}\mathrm{a}_e s_e+\sum_{e\in E(\Omega_c^C)\backslash E(\partial\Omega_c)}\mathrm{a}_e s_e\,,\quad(25)$$

$$\upsilon_s=\sum_{n\in N(\Gamma_h)}\upsilon_n,\quad(26)$$

where $E(\Omega_c)$ and $E(\Omega_c^C)$ are the set of element edges of Ω, s_e is the basic function linked to edge e, and a_e is the circulation of $\mathbf{a}$ along edge e in Ω. The $N(\Gamma_h)$ is the set of nodes defined in the BCs.

The association of equations (24), (25) and (26), the discreted equation is written as:

$$\int_\Omega\mu^{-1}\left(\mathrm{curl}\sum_{e\in E(\Omega_c)}\mathrm{a}_e s_e\cdot\mathrm{curl}\,\mathbf{w}'\right)d\Omega$$

$$+\int_\Omega\left(\mu^{-1}\sum_{e\in E(\Omega_c^C)\backslash E(\partial\Omega_c)}\mathrm{a}_e s_e\cdot\mathrm{curl}\,\mathbf{w}'\right)d\Omega$$

$$+\int_{\Omega_c}\sigma\sum_{e\in E(\Omega_c)}\mathrm{a}_e s_e\cdot\mathbf{w}'d\Omega_c$$

$$+\int_{\Omega_c}\left(\sigma\sum_{e\in E(\Omega_c^C)\backslash E(\partial\Omega_c)}\mathrm{a}_e s_e\cdot\mathbf{w}'\right)d\Omega_c$$

$$+j\int_{\Omega_c}\left(2\pi f\sigma\,\mathrm{grad}\sum_{n\in N(\Gamma_h)}\upsilon_n\cdot\mathrm{grad}\sum_i V_i v_{s,i}\right)d\Omega_c$$

$$=\int_\Omega(\mathbf{j_s}\cdot\mathbf{w}')d\Omega_s\quad(27)$$

5.   Numerical test

In this part, a test problem is a single-phase SR of 16 MVar and a voltage of $500/\sqrt{3}$ and freqency of 50 Hz. The electromagnetic parameters are now computed via the FEM, where the required results from the analytical approach are already given in Table 1. The geometry of a single phase SR is presented in Figure 4.
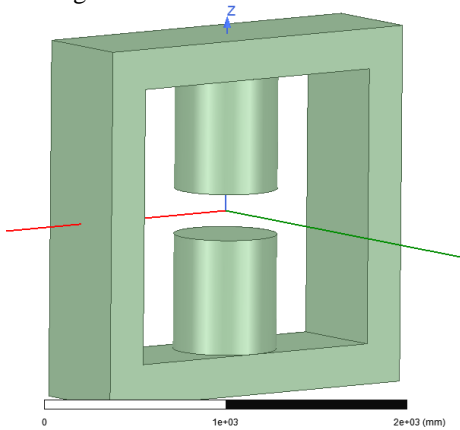
Figure 4. 3D model of a single phase high voltage SR.

The 3-D coarse mesh with edge and node elements is pointed out in Figure 5. The waveform of phase electric current distribution in the winding is shown in Figure 6. The distribution of magnetic vector potential due to the current flowing in the winding is presented in Figure 7. It can be seen that if the large air gap is divided into smaller air gaps, the fringing flux is evenly distributed in the flux air gaps along the core blocks and height of the winding without focussing on a single flux air gap. The maximum value reaches 1.226×10^{-7} (Wb/m).
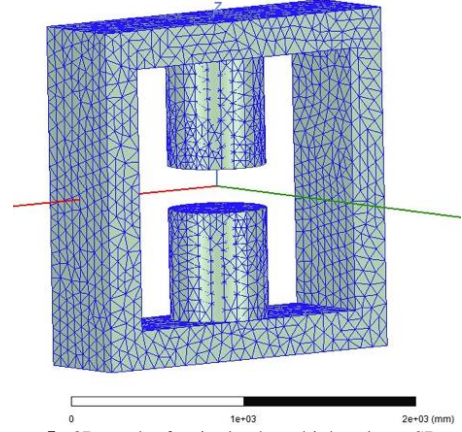
Figure 5. 3D mesh of a single phase high voltage SR.
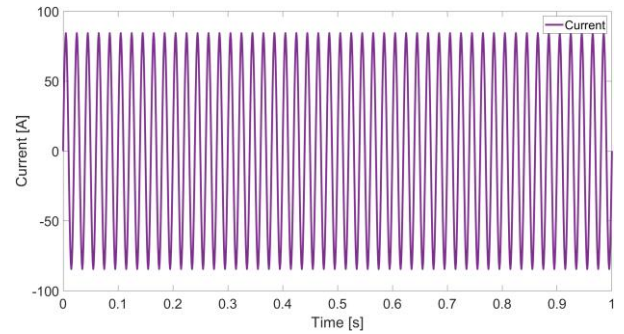
Figure 6. Waveform of electrical current distribution in the winding.
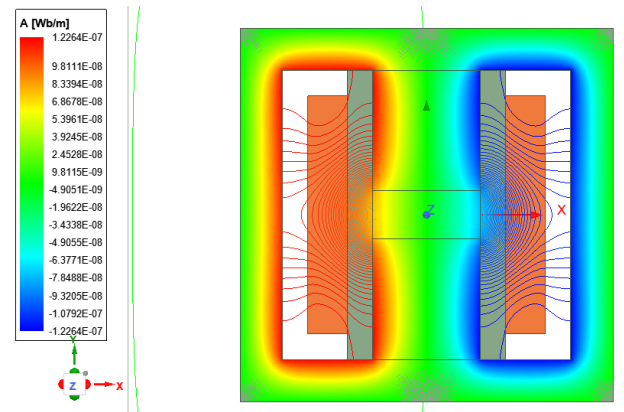
Figure 7. Distribution of magnetic flux density on B.

The distribution of fringing, air gap and total inductances is illustrated in Figure 8. The obtained results indicated that when the material used for the winding has a high permeability, and the air gap is sufficiently small, the flux density is mostly distributed in the core block without appearing the leakage or fringing flux. However, if the SR is designed with

one flux air gap intentionally at the core center with a large thickness, the magnetic flux leakage will be significant, resulting in a high reactive impedance and adversely affecting the performance of the magnetic core inductance [7]. Therefore, a large flux air gap divided into multiple smaller gaps will reduce the fringing and leakage flux along the core blocks. In order to overcome this difficulty as mentioned in [7], in this paper, instead of using a large flux air gap at the core center, it will be divided into five flux air gaps as shown in Figure 9.
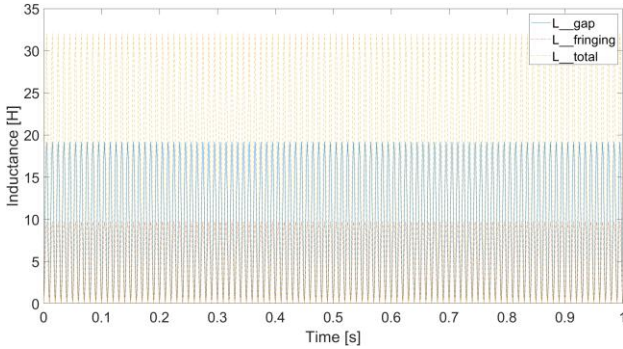
Figure 8. Distribution of air gap, fringing and total inductances.
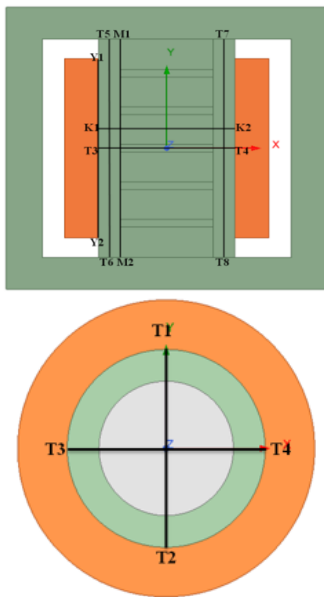
Figure 9. Model of the SR with five flux air gaps.

Figure 10 illustrates the distribution of magnetic flux density with five flux air gaps for the different positions along the winding and core blocks: T1T2, T3T4, T5T6, and T7T8. The magnetic flux density on the cut T5T6 decreases by 0.48 T compared to the case with a single air gap [7]. However, after five flux air gaps, this value mostly does not change.

Figure 11 presents the distribution of magnetic flux density along the segment Y1Y2 and M1M2. This result has indicated a variation in the percentage of leakage flux compared to the total flux value for the case of four flux air gaps (14 times). If the number of flux air gaps is increased to 5, the magnetic flux density along the segment Y1Y2 tends to be relatively uniform, and the leakage flux density through the air gaps significantly decreases.
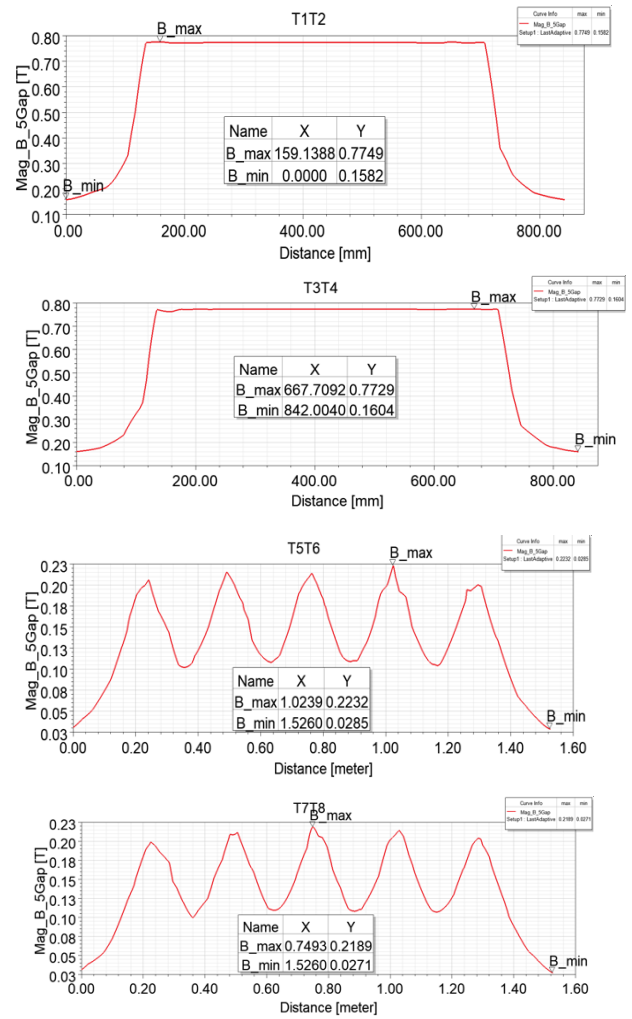
Figure 10. Distribution of magnetic flux density in air gaps along and across core blocks at the different positions T1T2, T3T4, T5T6 and T7T8 (see Figure 9).
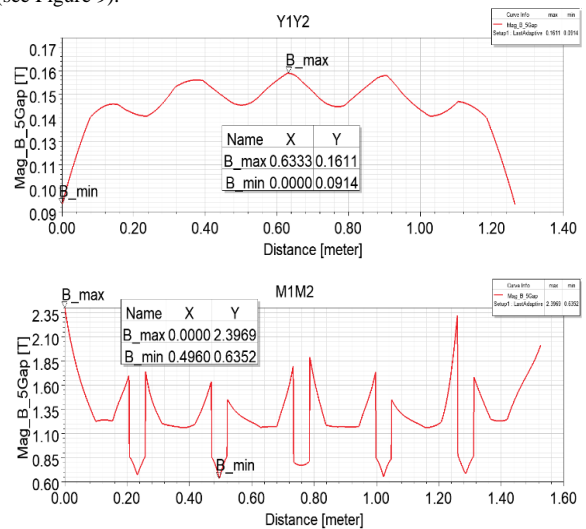
Figure 11. Distribution of magnetic flux density in air gaps and across core blocks at the different positions Y1Y2 and M1M2 (see Figure 9).

The distribution of electromagnetic force on the core blocks (K1K2) with five flux air gaps is pointed out in Figure 12. The value decreases by 1.03 times compared to the scenario with four flux air gaps, and this value remains relatively stable compared to the case with 4 air gaps (1.07 times).
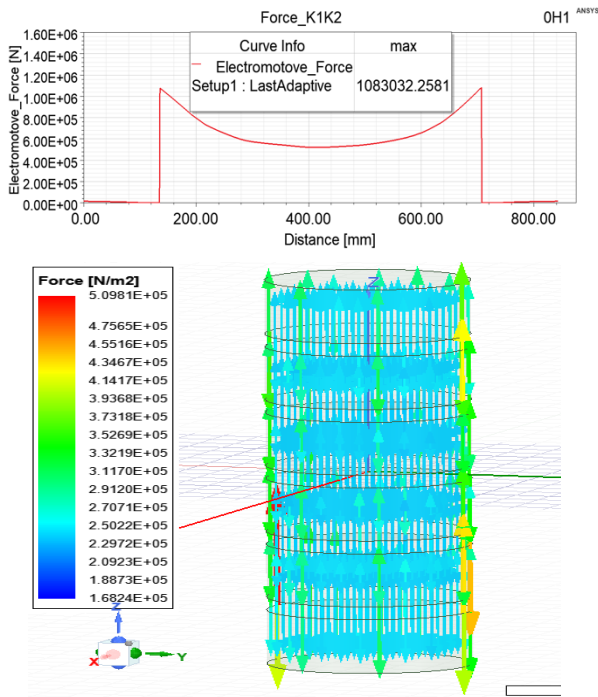
Figure 12. Distribution of electromagnetic force on the core block (K1K2) with five flux air gaps.

6. Conclusion

In this article, the combination of the two methods (analytical method and FEM) has been successfully developed for the single phase high voltage SR. The paper has investigated the distribution of magnetic vector potential in a single flux air gap, the magnetic flux density in five flux air gaps along and across the core blocks of the SR, and the electromagnetic forces acting on the core blocks as well. Via the simulated results, the division of the large flux air gap into the smaller air gaps has reduced the leakage and fringing flux in the flux air gaps. In particular, it can be shown that the electromagnetic forces acting on the upper and lower surfaces of the core blocks are in the same direction but opposite in magnitude, and approximately equal. Based on the obtained results, it will serve as reference data to assist designers and manufacturers to enhance and reinforce the structure of the partition plates between core blocks before production. Specifically, it has provided an appropriate choice of density for the steel core to reduce the electromagnetic forces acting on the surface of the core blocks and the surfaces of the partition plates between the core blocks. This will aid in optimizing the design and operation of SR to ensure the stability and performance of the electrical system.

References

[1]   Gagari Deb *"Ferranti Effect in Transmission Line"* International Journal of Electrical and Computer Engineering (IJECE) Vol.2, No.4, August 2012, pp. 447~451 ISSN: 2088-8708.

[2]   A. Divya Swarna Sri *"Depiction and Compensation of Ferranti Effect in Transmission Line"* International Journal for Research in Applied Science & Engineering Technology (IJRASET) ISSN: 2321-9653; Volume 6 Issue III, March 2018.

[3]   Tu Pham Minh, Hung Bui Duc and Vuong Dang Quoc. Analysis of Leakage Inductances in Shunt Reactors-Application to High Voltage Transmission Lines. Engineering, Technology & Applied Science Research (eISSN 1792-8036; pISSN 2241-4487), Vol. 12, no. 3, pp. 8488-8491 year 2022.

[4]   Tu P. Minh, Hung B. Duc, Tuan P. Anh and Vuong D. Quoc. A Novel Approach for the Modeling of Electromagnetic Forces in Air-Gap Shunt Reactors. Engineering, Technology & Applied Science Research (eISSN 1792-8036; pISSN 2241-4487), Vol. 12, no. 1, pp. 8223-8227.

[5]   Pham Minh Tu, Dang Quoc Vuong, and Bui Duc Hung. "Study of Number and Size of Air-Gaps in Core of Shunt Reactors in Tranmission Lines of High and Supper High Voltages". Journal of Military Science and Technology, no. 80, June 2022, pp. 23-30, doi:10.54939/1859-1043.j.mst.80.2022.23-30.

[6]   T. P. Minh, H. B. Duc, and V. D. Quoc, *"Analysis of Leakage Inductances in Shunt Reactors: Application to High Voltage Transmission Lines"*, *Eng. Technol. Appl. Sci. Res.*, vol. 12, no. 3, pp. 8488–8491, Jun. 2022.

[7]   Hung Bui Duc, Dung Dang Chi, Dang, Q.-V., & Anh Hoang. (2023). Computation of Electromagnetic Parameters of Shunt Reactors Taken Corner Chamfers of Core Block into Account. *Measurement, Control, and Automation*, *4*(2), 42-46. Retrieved from https://mca-journal.org/index.php/mca/article/view/186

[8]   A. Balakrishnan, W.T. Joines, T.G. Wilson, *"Air-gap reluctance and inductance calculations for magnetic circuits using a Schwarz-Christoffel transformation"* IEEE Transactions on Power Electronics 12 (July (4)) (1997) 654–663

[9]   Lü, Fangcheng & Guo, Jiayi & Niu, Leilei & Geng, Jianghai & Pan, Yirui *"A New 3D Method for Reactor Core Vibration Based on Silicon Steel Lamination Rules and Application in UHV Shunt Reactors"* Mathematical Problems in Engineering. 2019. 1-11. 10.1155/2019/7290536.

[10]   H. Amreiz, A. Janbey and M. Darwish, *"Emulation of Series and Shunt Reactor Compensation"* 2020 55th International Universities Power Engineering Conference (UPEC), 2020, pp. 1-6,   doi: 10.1109/UPEC49904.2020 .9209786.

[11]   D. I. Zaikin, S. Jonasen and S. L. Mikkelsen, *"An Air-Gap Shape Optimization for Fringing Field Eddy Current Loss Reductions in Power Magnetics"* in IEEE Transactions on Power Electronics, vol. 34, no. 5, pp. 4079-4086, May 2019, doi: 10.1109/TPEL.2018.28682 89.

[12]   S.V. Kulkarni, S.A. Khaparde *"Transformer Engineering: Design, Technology, and Diagnostics"* Second Edition, ISBN 9781439853771, Published October 10, 2012 by CRC Press.

[13]   Kamran Dawood *"Modeling of Distribution Transformer for Analysis of Core Losses of Different Core Materials Using FEM"* 2019 8th International Conference on Modeling Simulation and Applied Optimization (ICMSAO)

[14]   F. Yuan et al., "Thermal Optimization for Dry Type Air Core Reactor Base on FEM," 2018 21st International Conference on Electrical Machines and Systems (ICEMS), 2018, pp. 1726-1730, doi: 10.23919/ICEMS.2018.8549257.

[15]   S. Magdaleno-Adame, R. Escarela-Perez, J. C. Olivares-Galvan, E. Campero-Littlewood and R. Ocon-Valdez, *"Temperature Reduction in the Clamping Bolt Zone of Shunt Reactors: Design Enhancements,"* in IEEE Transactions on Power Delivery, vol. 29, no. 6, pp. 2648-2655, Dec. 2014, doi: 10.1109/TPWRD.2014.2322994.

[16]   Najafi, A., Iskender, I. "*Comparison of core loss and magnetic flux distribution in amorphous and silicon steel core transformers.* " Electr Eng 100, 1125–1131 (2018). doi:10.1007/s00202-017-0574-7

[17]   K. Dawood, G. Komurgoz and F. Isik, *"Modeling of Distribution Transformer for Analysis of Core Losses of Different Core Materials Using FEM,"* 2019 8th International Conference on Modeling Simulation and Applied Optimization (ICMSAO), 2019, pp. 1-5, doi: 10.1109/ICMSAO.2019.8880392.

        S. Koruglu, P. Sergeant, R.V. Sabarieqo, Vuong. Q. Dang, M. De Wulf *"Influence of contact resistance on shielding efficiency of shielding gutters for high-voltage cables,"* IET Electric Power Applications, Vol.5, No.9, (2011), pp. 715-720.